

# Flow Separation in Four Configurations of Three Tandem Minibus Models

Nasaruddin Salam, Rustan Tarakka, Jalaluddin, and Muh Annur Jimran  
Department of Mechanical Engineering, Hasanuddin University, Gowa, Indonesia  
Email: nassalam.unhas@yahoo.co.id, rustan\_tarakka@yahoo.com, jalaluddin\_had@yahoo.com, muhannurjimran@yahoo.com

Muhammad Ihsan  
Baramuli College of Engineering, Pinrang, Indonesia  
Email: m.ihsan@stt-baramuli.ac.id

**Abstract**—This paper presents an investigation of the pressure coefficients and flow separation in four configurations of three tandem minibus models through experiments and CFD simulations. The wind tunnel was used to measure the pressure distribution by installing 14 tapping positions around the three minibusses' walls, and then the tapings were connected to a manometer. The dimensions of each model are 121mm × 45mm × 43mm (length, width, and height), and the ratio between the model and prototype is 1:40. The models are manufactured from iron with a thickness of 1 mm. Car 1 and car 2 are arranged in series at a constant distance (L) of 121 mm, while car 3 is installed in parallel with car 1 and car 2 with varying distances according to the configurations. The distances in the Y and X direction are denoted as M and N, respectively. N is set constant for each configuration. For configuration I, N is 0 mm. Furthermore, for configuration II, III, and IV, N is set at 121 mm, 242 mm, and 363 mm, respectively. Each configuration is given 6 M changes, with a constant airflow velocity (U) of 20 m/s or 72 km/h. The research was done at the Reynolds number (Re) of 55,120, which showed a significant change in the flow separation characteristics of the four configurations. Most values of the optimum pressure coefficient are positive, where the flow separation is smaller at the same  $M/D=0.57$ , in the following configuration order III, II, I, and IV subsequently.

**Index Terms**—flow separation, pressure coefficient, three tandem minibus cars, four configurations

## I. INTRODUCTION

In designs, especially of vehicles and infrastructures, which include buildings and utilities, designing a good shape requires adequate consideration of wind forces. Reducing energy loss on fluid flow across arrays of objects should be the major factor considered when designing shapes or structures. This is achieved by ensuring the elimination or delay of flow separation and subsequently generating the favorable uniform flow.

Salam et al. [1] conducted an experimental research on pressure distribution of flow across triangular and square cylinders, at several Reynolds numbers,  $Re=48,708$ ;  $64,435$ ;  $94,480$ ;  $119,509$  and  $152,449$ . These Reynolds numbers were determined based on the diameter of square cylinders. The L/D ratios of distances between the two square cylinders to the hydraulic diameter of square cylinders were varied at 0.5, 1.0, and 1.5. The d/D ratio of hydraulic diameters of the triangular cylinder and square cylinders was constant at 0.5. The pressure distribution was analyzed using CFD. The numerical and experimental studies showed that the pattern of pressure distribution and the pressure coefficient around objects decreases with an increase in the L/D ratios. The minimum pressure coefficient is recorded at  $L/D=1.0$  for every Reynolds number.

Kant et al [2] analyzed the reduction in drag of a hatchback and a generic sedan using the CFD model. The review compared the effect of drag forces on the two vehicle types by applying various types of vortex generators and spoilers. The drag on the sedan was also compared with that of the hatchback type car. The coefficient of drag exhibited little variation concerning velocity, while there is a significant variation with the changing body shape.

Moussa et al. [3] applied rear suction in the study of aerodynamic drag on a generic SUV. They proposed a novel methodology which combines automatic modeling of suction slits, CFD model, and orthogonal arrays in the global search method to recognize the parameters responsible for achieving a maximum reduction in aerodynamic drag reduction. Their results established that a proper suction mechanism design was able to reduce drag by up to 9%.

Wahba et al. [4] simulated aerodynamic drag on ground vehicles using lateral guide vanes, based on Reynolds-averaged Navier-Stokes equations, and incorporating two-equation eddy viscosity models on turbulence closure. Optimal configuration for improved aerodynamic performance was achieved by varying chord length, guide vane cross-section, and the angle of attack. Simulations indicated an overall reduction of

aerodynamic drag of up to 18% for the bus and SUV models using lateral guide vanes.

Lamond et al. [5] studied drag reduction in bluff two-box SUVs. Their findings indicated that under a condition of deflected flow in the outlet, drag reduction escalates as the mass flow rate increases. A drop of about 2kg/s in mass flow rates could reduce the drag coefficient by 8.2%. This is achieved by controlling the turbulent wake to the rear part of the vehicle with a side part outlet. A less 1.5kg/s reduction in mass flow rate could contribute to drag reduction by 10.7%, and this can likewise be achieved by applying an outlet on the upper rear of the SUV.

Salam et al. [6] have also researched the impact of attaching inlet disturbance body towards drag through square cylinders arranged in tandem. Experimental results have shown the tendency to reduce drag and pressure coefficients with an increase in L/D and d/D.

Moreover, Mokhtar and Jahan [7] studied the aerodynamic flow around generic sports utility vehicles via the CFD model. This study focused on the flow around a generic SUV model based on the popular SUV models. Despite its simplicity, it included all the basic features of a modern Sports Utility Vehicle. The CFD study performed in this research incorporated the K- $\epsilon$  turbulence model with Reynolds Average Navier Stokes (RANS) equations. This study provided comprehensive information about the flow pattern around a generic SUV and aerodynamic drag and lift forces.

Singh et al. [8] also conducted a numerical investigation on a generic SUV model equipped with a drag reduction add-on device. The results showed that using the device caused an increase in the total base pressure on the SUV. A total reduction of 8% in the aerodynamic drag coefficient was reported on the application of an add-on device.

Hassan et al [9] also studied the aerodynamic drag reduction of racing cars using a numerical model. He focused on various aerodynamic drag aspects and drag reduction techniques using the finite volume method to solve the Favre-averaged Navier-Stokes equations supported by the k- $\epsilon$  turbulence model. It was shown that drag could be reduced up to 22.13% by varying rear under-body modifications and up to 9.5% by exhaust redirection.

Tarakka et al. [10] investigated the application of active suction control on vehicle models, varied in frontal slant angle of 25°, 30° and 35 using a computational and experimental approach. The highest increase in pressure coefficients, 26.50%, was found on a 35° slant angle. The maximum reduction of aerodynamic drag was also achieved on the same model, obtaining a value of 14.74 from CFD and 13.57 from experiments.

Brow and Fred [11] investigated the potential of reducing aerodynamic drag and fuel consumption. They reported an average fuel efficiency of about 6-7%. Sudin et al. [12] conducted a comprehensive review of some aerodynamic drag reduction methods. Overall, the aerodynamic drag is suspected to be responsible for up to 50% of the fuel consumption at expressway speeds.

Wang et al [13] conducted research on active flow control on 25° slant angle Ahmed body by applying a novel unsteady jet. The new control devices could produce up to 13.6% drag reduction. Roumeas et al. [14] researched drag reduction using a local suction system embedded on the upper part of the rear window. It was able to reduce aerodynamic drag by approximately 17%.

Salam et al. [15] conducted a research on flow separation across three tandem square cylinders with two distance arrangement; serial and parallel, which are designated as model I and II. Model I varied in M/D ratios of the distance between cylinder 1 and cylinder 2 to the hydraulic diameter of the cylinder and N/D constant ratio of the distance between cylinder 2 and cylinder 3 to hydraulic diameter of the cylinder. Similarly, Model II varied gradually in M/D and N/D. Results showed that flow separation could be dissipated in both models.

Sandrine et al. [16] investigated flow separation control on a generic ground vehicle by applying steady micro jets. Using an array of steady microjet, drag coefficients can be reduced by 9-14%. Wassen and Thiele [17] simulated the use of rear edge active separation control on a generic vehicle. Through Large Eddy Simulations, this actuation method can decrease the aerodynamic drag by 10.2%.

Based on the research results of Salam, et.al. [1][6][15], A reduction in the drag coefficient of tandem objects could be achieved by attaching a disturbance body and by varying the interaction between the two objects in terms of the distance and diameter. According to Cengel and Cimbala [18], the drag coefficient value for a minibus or minivan is 0.4. The question is, how much is the reduction in the drag coefficient and pressure coefficient of minibuses when arranged in tandem in various configurations. This could be an interesting topic, given the current density of vehicle traffic on the expressway.

## II. METHODOLOGY

The research combines experiments in a wind tunnel to measure the pressure distribution of flow and simulation using the CFD FLUENT 6.3 software. The pressure distribution was measured by installing 14 tapping positions around the wall of the investigated vehicle. The test objects were three metallic minibus models, 121 mm length, 45 mm width, and 43 mm height, 44 mm hydraulic diameter D, on a 1:40 ratio of a model to the real object.

The three models were arranged in four configurations where car 1 and car 2 were arranged in series at a constant distance L. The position of car 3 varied in the Y or sideward direction at the distance of M, as well as in the X or forward direction at a distance of N depending on the configuration. The N distance was constant for each configuration. It was set at 0 mm for configuration I, 121 mm for configuration II, 242 mm for configuration III, and 363 mm for configuration IV.

The ratio N/D was set at N/D=0 for configuration I (car 3 parallel to car 2), N/D=2.75 for configuration II (car 3 parallel in between car 1 and car 2), N/D= 5.5 for

configuration III (car 3 parallel to car 1), and  $N/D=8.25$  for configuration IV (car 3 parallel and ahead to car 1). Every configuration model was given 6 variations in  $M$  distances (25mm, 50mm, 75mm, 100mm, 125mm, and 150mm). They were also assigned the same level of

upstream flow speed of 20 m/s. Fig. 1 shows the position of the three models in four configurations with six levels of  $M/D$  ratios (0.57, 1.13, 1.70, 2.27, 2.84, and 3.41) and four levels of  $N/D$  ratios (0.0, 2.75, 5.50, and 8.25) as well as a constant  $L/D$  ratio of 2.75.

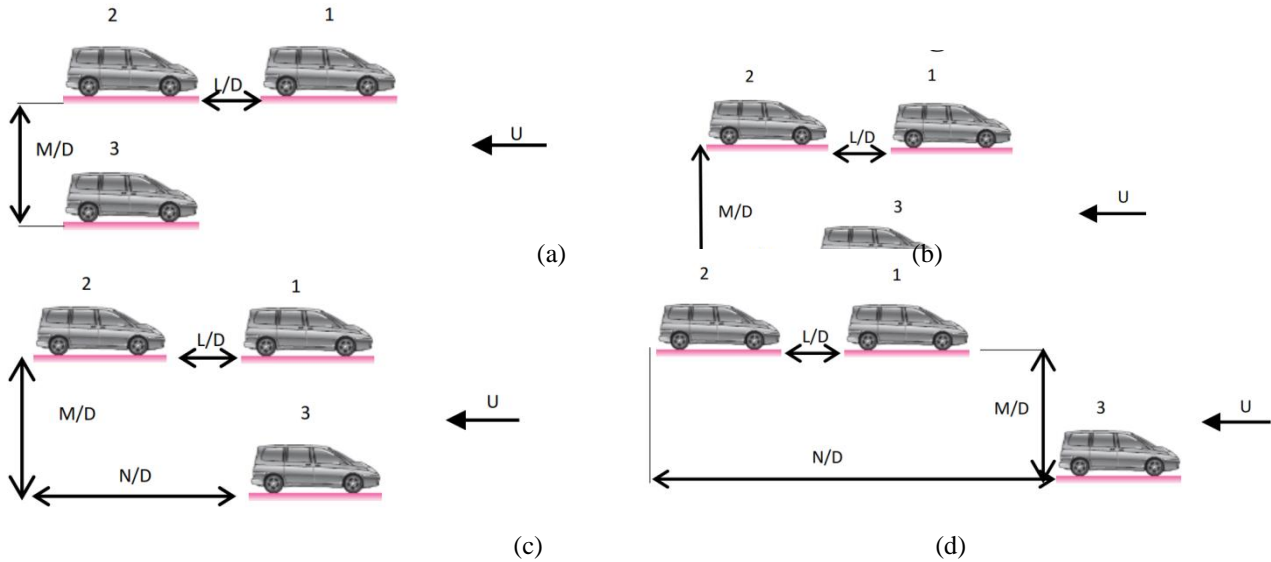


Figure 1. Tandem arrangement of 3-minibus in four configuration (a) configuration I, (b) configuration II, (c) configuration III and (d) configuration IV

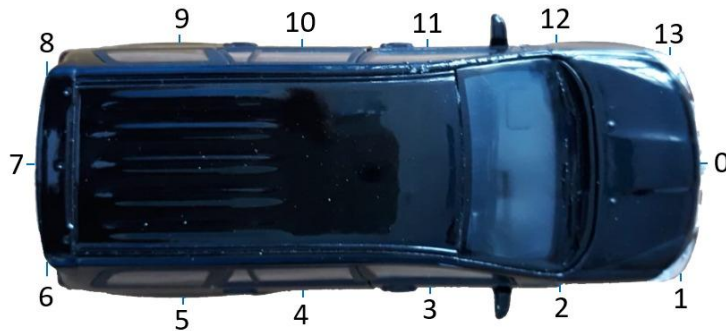


Figure 2. Taping positions on minibus model

The wind tunnel employed in the study is a low-speed wind tunnel manufactured by Plint & Partners LTD Engineers [19]. The maximum air velocity through a 300 mm x 300 mm test section is determined at 22 m/s

Cengel et al. [18] determined the formula of the drag coefficient and described the characteristics of fluid flow across a minibus, the Reynolds ( $Re$ ) formula shown in Eq. 1 was used,

$$Re = \frac{U \cdot D}{\nu} \quad (1)$$

The variables and parameters in the equation above are upstream air velocity ( $U$ ), the hydraulic diameter of minibus models ( $D$ ), and the kinematic viscosity of the air ( $\nu$ ).

In determining the pressure coefficient ( $C_p$ ), the following equation, Eq. 2 was, used,

$$C_p = \frac{h_{sm} - h}{h_{sm} - h_{tm}} \quad (2)$$

The variables in equation (2) include the static head at each tapping point around the models ( $h$ ), the static head of the airflow manometer before passing the models ( $h_{sm}$ ), and the total head of the pitot tube air flow manometer before passing the models ( $h_{tm}$ ). Kinematic air viscosity is determined by pressure conditions at room temperature of the laboratory.

The experiment was conducted in a laminar flow regime or  $Re < 10^5$ , specifically at  $Re = 55,120$ , based on the length and the hydraulic diameter of the minibus model. Air velocity was kept constant at 20 m/s,

### III. RESULTS AND DISCUSSION

Results are obtained from the experiment as the values of pressure coefficients at tapping positions on the circumference of the minibus model where the flow separation occurred. Tables I, II, III, and IV show the pressure coefficients on the minibus model for each configuration. The obtained pressure coefficients were

then compared to the four tapping position for each side of the minibus model, that is, the front wall of the minibus model (Tp0), the right wall of the minibus model, the cylinder (Tp3), the rear wall of minibus model (Tp7) and the left wall of minibus model (Tp11), as shown in Fig. 2, at Re=55,120.

Table I shows the characteristics of flow separation of each minibus model for configuration I, with varied M/D from 0.57 to 3.41 and constant N/D of 0.0 on Re=55,120. Table I also shows that the position of car 1 toward car 2

on L/D=2.75 dampens the flow separation on car 2. On the rear wall of car 2 or on tapping position Tp7, there is no separation at all, as indicated by a positive Cp on all tapping position. Likewise, for the position of car 3 to car 2, the smaller the M/D or, the closer car 3 is to car 2, the smaller the flow separation on car 3. In that position, the smallest separation occurs on M/D=2.27 and M/D=2.28. Based on this phenomenon, it is suggested that when car 3 is beside car 2, the optimum positions are in between.

TABLE I. PRESSURE COEFFICIENT (Cp) OF THE TANDEM THREE MINIBUS CONFIGURATION I WITH M/D VARYING FROM 0.57 TO 3.41 WHILE N/D IS CONSTANT AT 0.0 AND AT TAPPING POSITIONS Tp0, Tp3, Tp7 & Tp11 ON CAR 1 (C1), CAR 2 (C2), AND CAR 3 (C3), AT RE = 55,120.

M/D	Car 1 (C1)				Car 2 (C2)				Car 3 (C3)			
	Tp0	Tp3	Tp7	Tp11	Tp0	Tp3	Tp7	Tp11	Tp0	Tp3	Tp7	Tp11
0.57	0.9	-2.1	-1.6	-1.6	3.4	0.1	0.4	0.6	0.5	-0.6	-0.5	-0.6
1.13	0.5	-6.5	-5.3	-5.3	7.0	-2.0	1.0	1.0	-0.5	-2.7	1.0	-2.7
1.70	0.9	-1.9	-1.5	-1.5	2.8	-0.1	0.3	0.4	-1.0	-3.4	-3.4	-3.4
2.27	0.9	-1.9	-1.5	-1.5	2.9	0.1	0.3	0.4	0.5	-0.4	-0.5	-0.4
2.84	0.9	-2.1	-1.6	-1.6	3.1	0.1	0.3	0.4	0.6	-0.4	-0.5	-0.4
3.41	0.6	-8.2	-6.4	-6.4	3.2	0.2	0.3	0.4	0.3	-0.8	-0.8	-0.8

Table II illustrates the flow separation characteristics of the respective minibus model for Configuration II, where M/D varies from 0.57 to 3.41 and N/D=2.75 on constant Reynolds Re=55,120. From table 2, It can be seen that the position of car 1 against car 2 at L/D=2.75 causes no flow separation in general for car 2. This is indicated by a positive Cp value at all tapping positions, except at M/D=1.13. Likewise, at the position of car 3 towards car 2 and car 1, the smaller the M/D value or the

closer car 3 is to car 2 and car 1, the smaller the flow separation will be on car 3. The smallest flow separation is observed at M/D=2.27. Based on this phenomenon, when car 3 is on the side between car 2 and car 1, the lowest CP value is at M/D=1.13 and M/D=1.70.

Table III presents the characteristics of flow separation for each car on configuration III, as M/D ratios varied from 0.57 to 3.41, and the N/D ratio is set to a constant 5.50 at a constant Re=55,120.

TABLE II. THE PRESSURE COEFFICIENT (Cp) OF THE TANDEM THREE MINIBUS CONFIGURATION II CARS WITH M/D CHANGING FROM 0.57 TO 3.41 WHILE N/D IS CONSTANT AT 2.75 AND AT TAPPING POSITIONS Tp0, Tp3, Tp7 & Tp11 ON CAR 1 (C1), CAR 2 (C2) AND CAR 3 (C3), AT RE=55,120.

M/D	Car 1 (C1)				Car 2 (C2)				Car 3 (C3)			
	Tp0	Tp3	Tp7	Tp11	Tp0	Tp3	Tp7	Tp11	Tp0	Tp3	Tp7	Tp11
0.57	0.9	-1.8	-1.4	-1.3	2.7	0.4	0.4	0.5	0.6	-0.4	-0.4	-0.3
1.13	0.5	-6.2	-5.2	-5.2	4.7	-1.7	-1.2	-1.0	-0.3	-2.7	-2.5	-2.3
1.70	0.9	-1.9	-1.4	-1.4	2.7	0.1	0.3	0.3	-0.3	-2.7	-2.8	-2.7
2.27	0.9	-1.8	-1.3	-1.3	2.6	0.1	0.3	0.4	0.6	-0.3	-0.4	-0.3
2.84	0.9	-1.9	-1.4	-1.3	2.7	0.3	0.4	0.5	0.6	-0.4	-0.4	-0.3
3.41	0.6	-5.6	-4.6	-4.4	2.8	0.3	0.4	0.4	0.4	-0.7	-0.7	-0.7

TABLE III. TANDEM PRESSURE COEFFICIENT (Cp) OF THE TANDEM THREE MINIBUS CONFIGURATION III WITH M/D CHANGING FROM 0.57 TO 3.41 WHILE N/D IS CONSTANT AT 5.50 AND AT TAPPING POSITIONS Tp0, Tp3, Tp7 & Tp11 AT CAR 1 (C1), CAR 2 (C2) AND CAR 3 (C3), AT RE=55,120.

M/D	Car 1 (C1)				Car 2 (C2)				Car 3 (C3)			
	Tp0	Tp3	Tp7	Tp11	Tp0	Tp3	Tp7	Tp11	Tp0	Tp3	Tp7	Tp11
0.57	0.9	-2.1	-1.4	-1.5	2.6	0.2	0.5	0.6	0.4	-0.3	-0.3	-0.3
1.13	0.9	-2.3	-1.5	-1.5	2.7	0.3	0.5	0.6	-0.7	-2.5	-2.5	-2.5
1.70	0.9	-2.2	-1.5	-1.5	2.6	0.1	0.3	0.5	-0.3	-1.6	-1.6	-1.6
2.27	0.9	-2.2	-1.5	-1.5	2.5	0.2	0.3	0.5	0.4	-0.3	-0.3	-0.3
2.84	0.9	-2.2	-1.5	-1.4	2.7	0.3	0.5	0.5	0.5	-0.5	-0.4	-0.3
3.41	-0.3	-4.8	-4.0	-4.0	2.8	0.4	0.5	0.6	0.3	-0.7	-0.7	-0.7

From Table III, it is shown that the position of car 1 to car 2 at L/D=2.75 stops the flow separation on car 2 as indicated by the positive Cp value of all tapping positions. Likewise, for the position of car 3 towards car 1, the smaller the value of M/D or the closer car 3 is to car 1, the smaller the flow separation for car 3, and the smallest flow separation is observed at M/D=0.57 and M/D=2.27. Based on these findings, when car 3 is beside car 1, the

position of car 3 that needs to be avoided is at M/D=1.13 because the largest flow separation is observed there.

Table IV shows the characteristics of flow separation for models in configuration IV, as the M/D ratio varied from 0.57 to 3.41, and N/D=8.25 is set constant, at the constant Reynolds number of Re=55,120

TABLE IV. TANDEM PRESSURE COEFFICIENT (Cp) OF THE TANDEM THREE MINIBUS CONFIGURATION IV WITH M / D CHANGING FROM 0.57 TO 3.41 WHILE THE N/D IS CONSTANT AT 8.25 AT THE TAPPING MEASUREMENT POSITIONS TP0, TP3, TP7 & TP11 AT CAR 1 (C1), CAR 2 (C2) AND CAR 3 (C3), AT Re = 55,120.

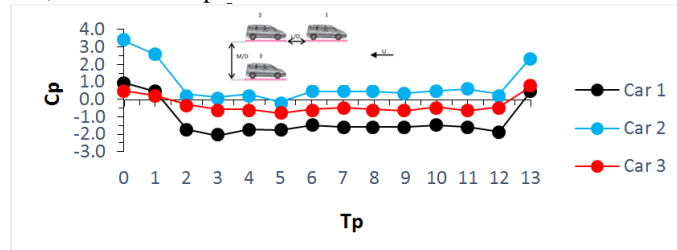
M/D	Car 1 (C1)				Car 2 (C2)				Car 3 (C3)			
	Tp0	Tp3	Tp7	Tp11	Tp0	Tp3	Tp7	Tp11	Tp0	Tp3	Tp7	Tp11
0.57	0.9	-1.9	-1.3	-1.4	2.5	0.4	0.5	0.6	-0.1	-0.3	-0.3	-0.3
1.13	0.6	-5.9	-4.4	-4.9	5.6	-1.0	-0.6	-0.4	-1.6	-2.0	-2.0	-2.0
1.70	0.9	-2.1	-1.6	-1.7	2.7	0.4	0.5	0.7	-2.8	-3.4	-3.2	-3.2
2.27	0.9	-1.9	-1.4	-1.5	2.6	0.3	0.4	0.5	-0.1	-0.3	-0.3	-0.3
2.84	0.9	-2.1	-1.5	-1.5	2.7	0.4	0.6	0.7	-0.1	-0.3	-0.3	-0.3
3.41	0.3	-10.8	-9.0	-9.0	2.6	0.3	0.5	0.6	-0.4	-0.6	-0.6	-0.7

From Table IV, it is obtained that the position of car 1 in relation to car 2 at L/D =2.75 causes car 2 to experience zero flow separation as indicated by the positive Cp value of all tapping positions, except at M/D=1.13. Likewise, for the position of car 3 in relation to car 1, the smaller the value of M/D or the closer car 3 is to car 1, the smaller the flow separation for car 3, and the smallest flow separation is observed at M/D=0.57, M/D=2.27, and M/D=2.84. Based on this results, the position that gives the largest CP value when car 3 is beside car 1 is at M/D=1.70.

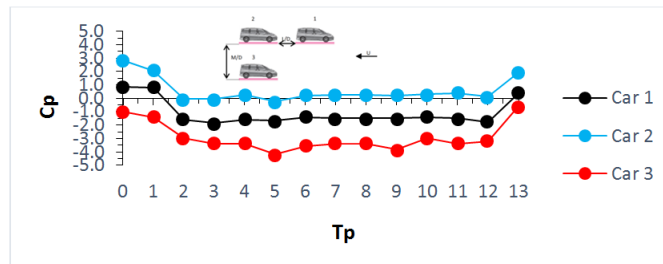
From the results of the flow separation shown in Table I to Table IV, the tandem of three minibusses reduces the flow separation, which consequently reduces flow resistance. When the flow separation review focuses on the flow separation of car 2, the flow separation is

dampened due to changes in the position of car 3 in the X direction (N/D) and the Y direction (M/D) for all configuration models. Likewise, if the flow separation view focuses on the flow separation of car 3, then the flow separation is dampened due to changes in the position of the distance between car 3 and car 2 in the X direction (N/D) and in the Y direction (M/D). It can also be seen that for the four configuration models, the configuration model II gives the lowest flow separation value.

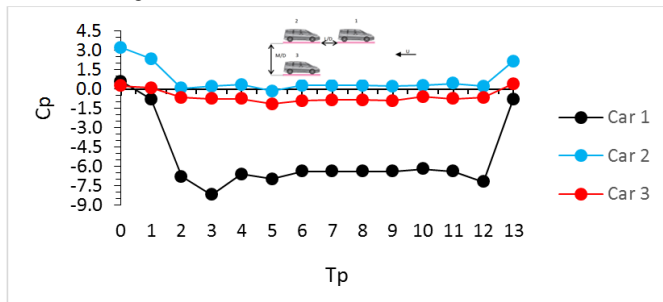
Figs. 3,4,5 and 6 show the corresponding relation of pressure coefficients (Cp) and the tapping position (Tp) on car 1, car 2 and car 3, for all configuration models at 3 levels of changing M/D, namely 0.57; 1.70 and 3.41; at constant Re=55,120.



(a) Configuration I (N/D = 0.0), M/D = 0.57at Re = 55,120



(b) Configuration I (N/D = 0.0), M/D = 1,70at Re = 55.120



(c) Configuration I (N/D = 0.0), M/D = 3,41at Re = 55.120

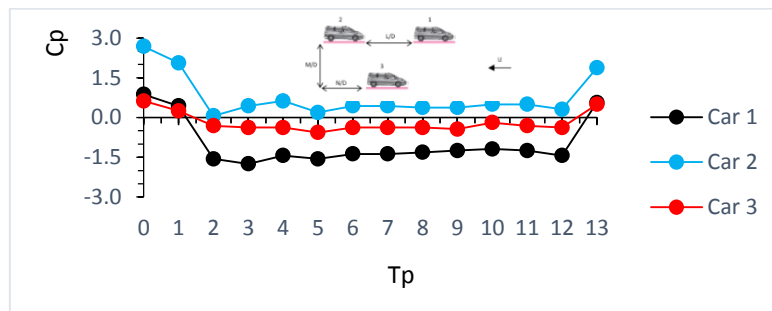
Figure 3.The relationship of the pressure coefficient (Cp) with the position of measurement points for cars 1, 2 and 3 configuration models I (N/D=0.0), (a) M/D=0.57, (b) M/D=1.70 and (c) M/D=3.41 at Re=55,120

Fig. 3 shows the relationship between pressure coefficients ( $C_p$ ), measurement point positions for car 1, car 2, and car 3 at  $Re=55,120$  in the configuration I arrangement and using three  $M/D$  ratios, which are (a)  $M/D=0,57$ , (b)  $M/D=1.7$  and (c)  $M/D=3.41$ .

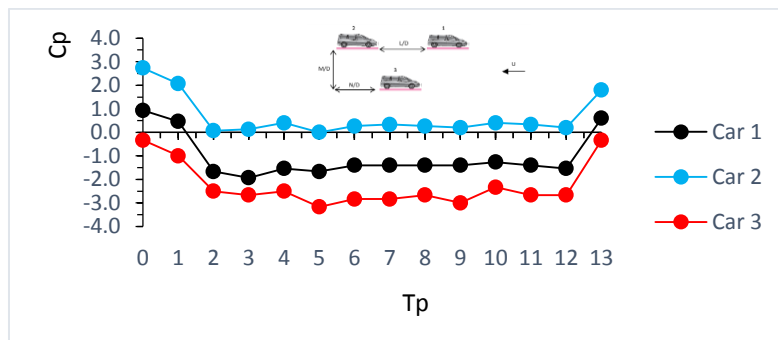
Fig. 3 (a) shows the presence of high intensity flow separation on car 1, where no flow separation was observed on car 2 except for  $Tp5$ , and on car 3, smaller flow separation was observed with a smaller  $C_p$  than those on car 1. Fig. 3 (b) shows high intensity flow separation on car 3, a dampened flow separation for car 2, and for car 1, there are smaller flow separations than that of car 3. Fig. 3 (c) shows intense flow separation on car 1

except at position  $Tp0$ , where no flow separation occurred. On car 2, flow separations are dampened, where there is no flow separation except for  $Tp5$ , while on car 3 there are flow separations, although smaller when compared to car 1.

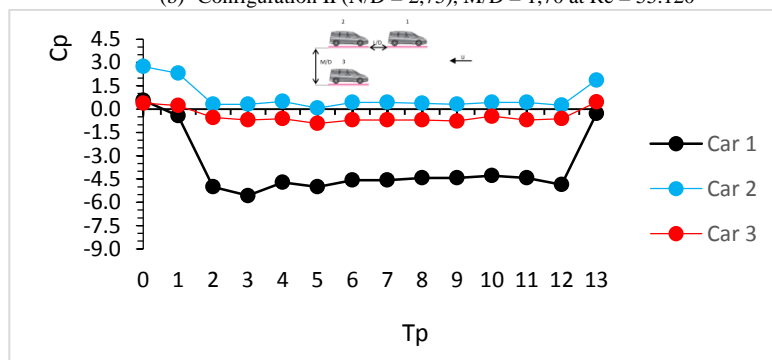
According to results shown on Fig. 3, the characteristics of the three tandem minibus model on configuration I show that the distance between car 1 and car 2 which is fixed ( $L/D=2.75$ ) and the change in position of car 3 to the Y axis (change in  $M/D$ ) and the position of car 3 on the X axis ( $N/D=0.0$ ) reduces the flow separation, where the largest dampening effect is recorded at  $M/D=0.57$ .



(a) Configuration II ( $N/D = 2,75$ ),  $M/D = 0,57$  at  $Re = 55.120$



(b) Configuration II ( $N/D = 2,75$ ),  $M/D = 1,70$  at  $Re = 55.120$



(c) Configuration II ( $N/D = 2,75$ ),  $M/D = 3,41$  at  $Re = 55.120$

Figure 4.Relation of the pressure coefficient ( $C_p$ ) with the measurement point positions of cars 1, 2 and 3 in configuration II arrangement ( $N/D=2.75$ ), (a)  $M/D=0.57$ , (b)  $M/D=1.70$  and (c)  $M/D=3.41$  at  $Re = 55,120$

Fig. 4 shows the relationship between pressure coefficients ( $C_p$ ) and the measurement point positions for car 1, car 2, and car 3 at  $Re = 55,120$  in the configuration model II arrangement. Figure 4 (a) shows intense flow

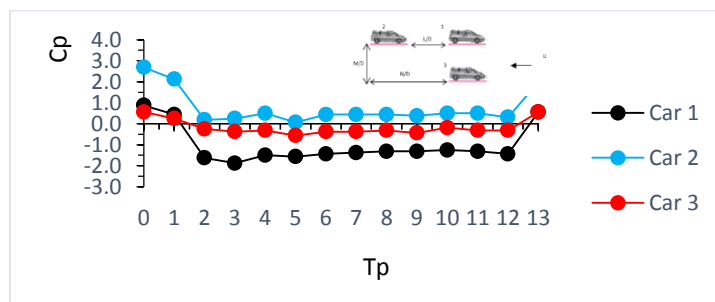
separation on car 1, while on car 2, there is no flow separation or all  $C_p$  values are positive. Similarly, on car 3, there is flow separation with smaller  $C_p$  than that of car 1. Fig. 4 (b) shows intense flow separation on car 3,

while on car 2, the flow separation is dampened, and all CP values are positive, showing no separation. On car 1, there is also flow separation but with smaller CP. Fig. 4 (c) shows intense flow separation on car 1, while on car 2, the flow separation is dampened, and all CP values are positive, indicating no flow separation. On car 3, there is flow separation, but the Cp value is smaller compared to car 1.

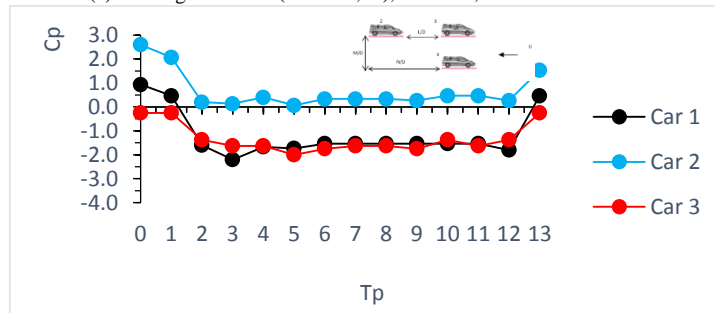
Based on Fig. 4, the characteristics of the three tandem minibus model configuration II show that the fixed position of the distance between car 1 and car 2 ( $L/D=2.75$ ), the fixed position of car 3 on the X axis ( $N/D=2.75$ ), and the varying position of the distance between car 3 and car 1 on the Y axis ( $M/D$ ) dampens the

flow separation. The highest damping effect is recorded at  $M/D=0.57$

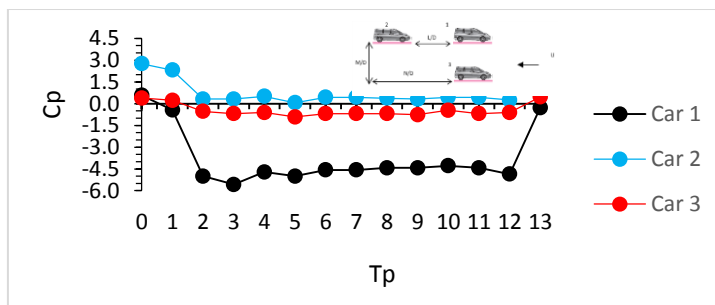
Fig. 5 shows the relation of pressure coefficients ( $C_p$ ) and the measurement point positions of car 1, car 2, and car 3 at  $Re=55,120$ , of three tandem minibus models in configuration III arrangement and at three levels of  $M/D$  ratio. (a)  $M/D=0.57$ , (b)  $M/D=1.70$  and (c)  $M/D=3.41$ . Figure 5 (a) shows an intense flow separation on car 1, while on car 2, the flow separation is dampened, and there is no flow separation. Figure 5 (b) shows an intense flow separation on car 1 and car 3, while on car 2, the flow separation is dampened, and there is no flow separation, whereas, on car 3, there is a flow separation that is greater than that observed in car 1.



(a) Configuration III ( $N/D = 5,50$ ),  $M/D = 0,57$  at  $Re = 55.120$



(b) Configuration III ( $N/D = 5,50$ ),  $M/D = 1,70$  at  $Re = 55.120$



(c) Configuration III ( $N/D = 5,50$ ),  $M/D = 3,41$  at  $Re = 55.120$

Figure 5. The relationship of the pressure coefficient ( $C_p$ ) with the measurement point ratings of cars 1, 2, and 3 measurement models III ( $N/D=5.50$ ), (a)  $M/D=0.57$ , (b)  $M/D=1.70$ , and (c)  $M/D=3.41$  at  $Re=55,120$

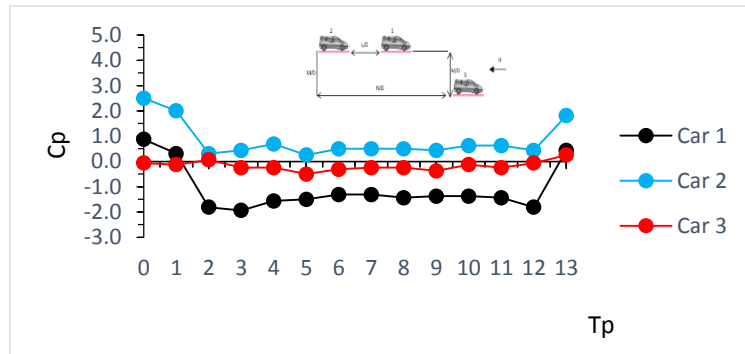
Fig. 5 (c) shows an intense flow separation on car 1, while on car 2, the flow separation is dampened, and no flow separation is observed, whereas on car 3, there is flow separation, but the flow separation is minimal compared to that of car 1.

Based on Fig. 5, the tandem characteristics of the three minibus models of configuration III indicate that the fixed position of the distance between car 1 and car 2 is ( $L/D=2.75$ ), the fixed position of car 3 on the X axis ( $N/D=5.50$ ), and the varying position of the distance

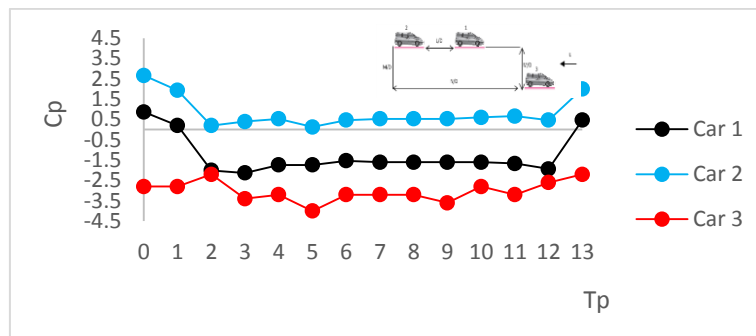
between car 3 and car 1 on the Y axis (M/D), dampens the flow separation. The most significant damping effect is recorded at M/D=0.57.

Fig. 6 shows the relationship between the pressure coefficient (Cp) and the position of tapping points for car 1, car 2 and car 3 at Re=55,120, for three tandem minibus model arranged according to configuration IV at a

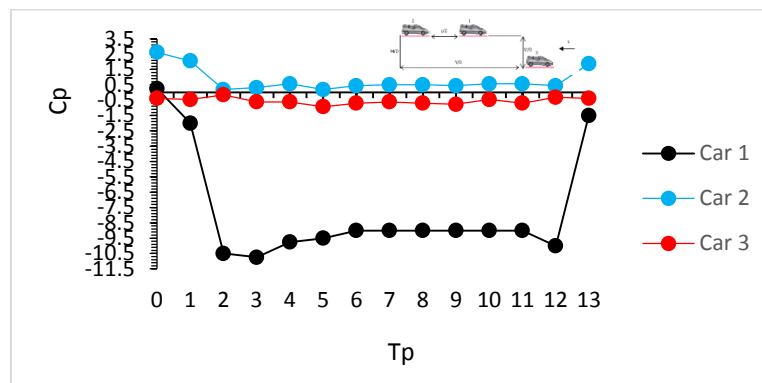
constant N/D ratio of 8.25, and three M/D ratios, which are (a) M/D=0.57, (b) M/D=1.70 and (c) M/D=3.41. Fig. 6 (a) shows intense flow separation on car 1, while on car 2, the flow separation is dampened and no flow separation is observed. On car 3 however, there is flow separation with smaller Cp value than that of car 1.



(a) Configuration IV (N/D = 8,25), M/D = 0,57 at Re = 55.120



(b) Configuration IV (N/D = 8,25), M/D = 1,70 at Re = 55.120



(c) Configuration IV (N/D = 8,25), M/D = 3,41 at Re = 55.120

Figure 6. The relationship between the pressure coefficient (Cp) and the measurement point positions of cars 1, 2 and 3 in configuration IV arrangement (N / D = 8.25), (a) M / D = 0.57, (b) M / D = 1.70 and (c) M / D = 3.41 at Re = 55,120

Fig. 6(b) shows intense flow separation on car 3, while on car 2, there is no flow separation. On car 1, there is a flow separation with a Cp value that is smaller than that of car 3. Figure 6(c) shows intense flow separation on car 1, while on car 2, there is no flow separation, whereas, on car 3, there is a flow separation with a smaller Cp value than on car 1.

Based on Fig. 6, the characteristics of the three tandem minibus models for configuration IV show that the fixed position of the distance between car 1 and car 2 (L/D=2.75), the fixed position of car 3 on the X axis (N/D=8.25), and the changing position of the distance between car 3 and car 1 on the Y axis (M/D), dampens

the flow separation. The largest effect is recorded at  $M/D=0.57$ .

Figs. 7, 8, 9, and 10 show the numerical simulation results from a top view of three tandem minibus cars with four configuration models. The figures show: (a) contours of pressure, (b) contours of velocity magnitude, (c) contours of stream function, and (d) contours of vorticity as obtained by the FLUENT 6.3 application, at  $L/D=1.375$  and  $M/D=0.57$  with a flow rate of  $U=20$  m/s. This result is compared to the experimental results

presented in Figs. 3 to 6, which show the flow separation of the three tandem minibus models. Fig. 7 shows the tandem of three minibusses in model I configuration. In Fig. 7(a) it can be seen that there are pressure increase on the front side of car 1, which drastically decreases on the left, right, and rear part of car 1, while on car 2 there is a decrease in pressure on the left and back, while the front and right sides of the car 2 seems to be stable.

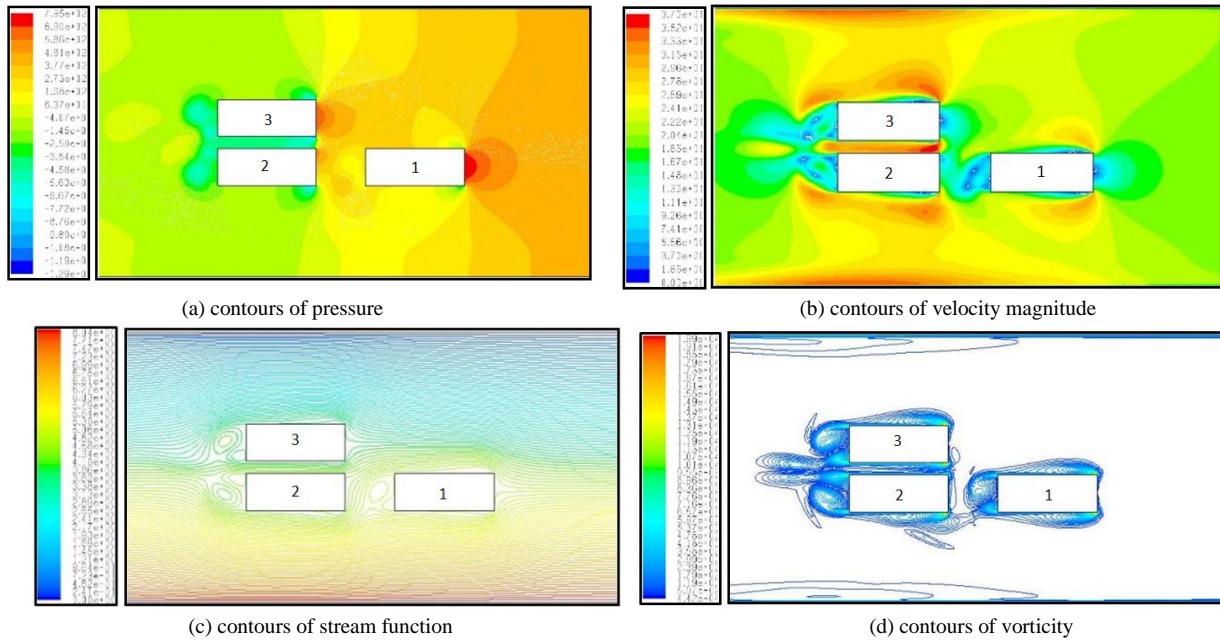
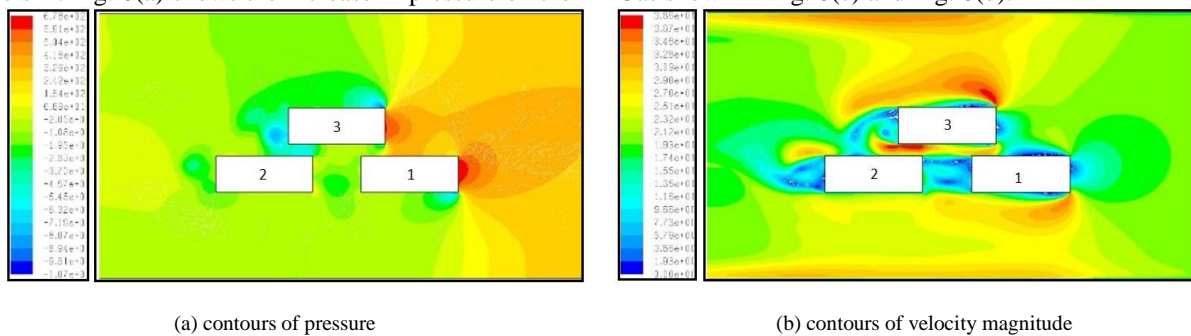


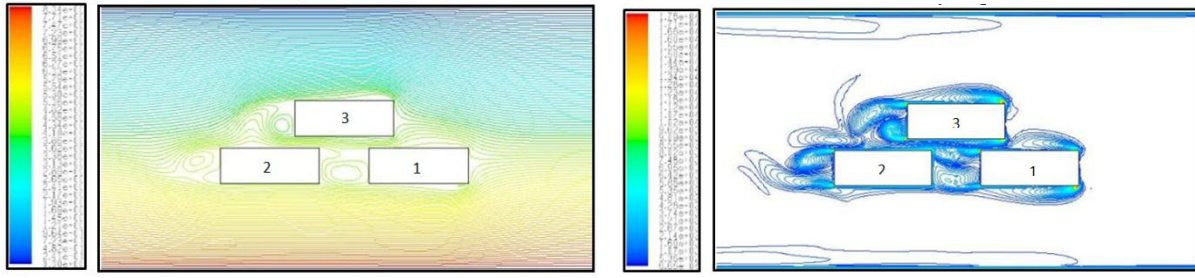
Figure 7. CFD simulation at  $U=20$  m/s ( $Re=55,120$ ),  $L/D=1.375$  and  $M/D=0.57$  of tandem three minibus car in model I configuration showing (a) contours of pressure, (b) contours of velocity magnitude, (c) contours of stream function, and (d) contours of vorticity.

Fig. 7(b) shows that the flow separation causes the boundary layer to be pushed upwards so that the thickness of the boundary layer increases, both on car 1 and car 3. It also shows an intense vortex behind car 2 and car 3, as shown in Fig. 7(c). Fig. 7(d) shows the presence of vortices starting from the left and right sides of car 1, car 2, and car 3 to the rear side of car 2 and car 3.

Fig. 8 shows a tandem of three minibus configuration models II. Fig. 8(a) shows the increase in pressure on the

front side of car 1 and car 3, which drastically decreases on the left and rear of car 3, while on car 2, there is a decrease in pressure on the left side, with the front and right side of car 2 appearing stable. In Fig. 8(b), the flow separation is shown to cause the boundary layer to be pushed upwards so that the thickness of the boundary layer increases for both car 1 and car 3. It also resulted in a relatively large vortex at the rear part of car 2 and car 3 as shown in Fig. 8(c) and Fig. 8(d).

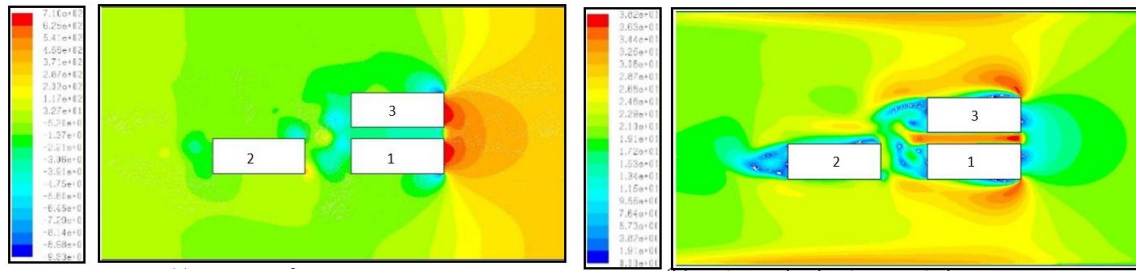




(c) contours of stream function

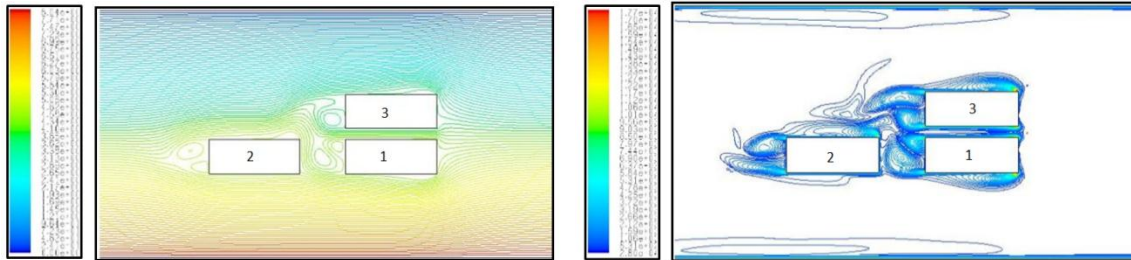
(d) contours of vorticity

Figure 8. CFD simulation at  $U=20$  m/s ( $Re=55,120$ ),  $L/D=1.375$ , and  $M/D=0.57$  of tandem three minibus car in model II configuration showing: (a) contours of pressure, (b) contours of velocity magnitude, (c) contours of stream function, and (d) contours of vorticity.



(a) contours of pressure

(b) contours of velocity magnitude



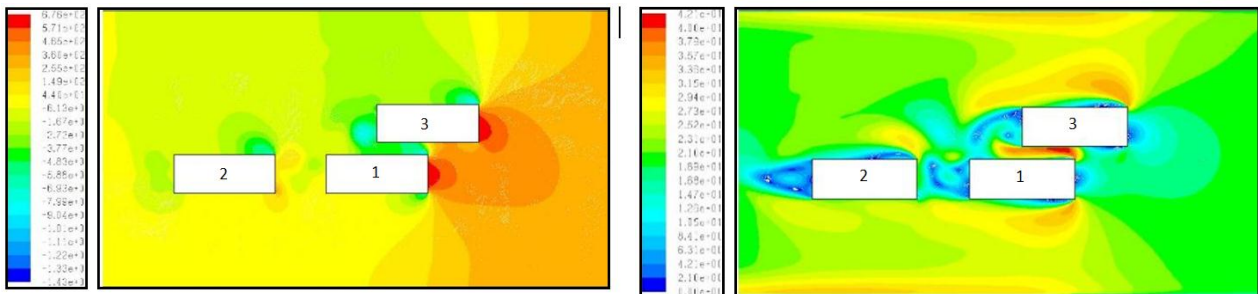
(c) contours of stream function

(d) contours of vorticity

Figure 9. CFD simulation at  $U=20$  m/s ( $Re=55,120$ ),  $L/D=1.375$  and  $M/D=0.57$  tandem three minibus cars in model III configuration showing: (a) contours of pressure, (b) contours of velocity magnitude, (c) contours of stream function, and (d) contours of vorticity

Fig. 9 shows configuration III. In Fig. 9(a), it can be seen that there is a significant increase of pressure on the front wall of car 1 and car 3, before drastic reduction on the left, right, and rear of car 1 and car 3, while on car 2,

it is more stable. Fig. 9(b) shows a small flow separation, both on car 1, car 2, and car 3. Also, small vortices are observed behind car 2 and car 3, as shown in Fig. 9(c) and Fig. 9(d).



(a) contours of pressure

(b) contours of velocity magnitude

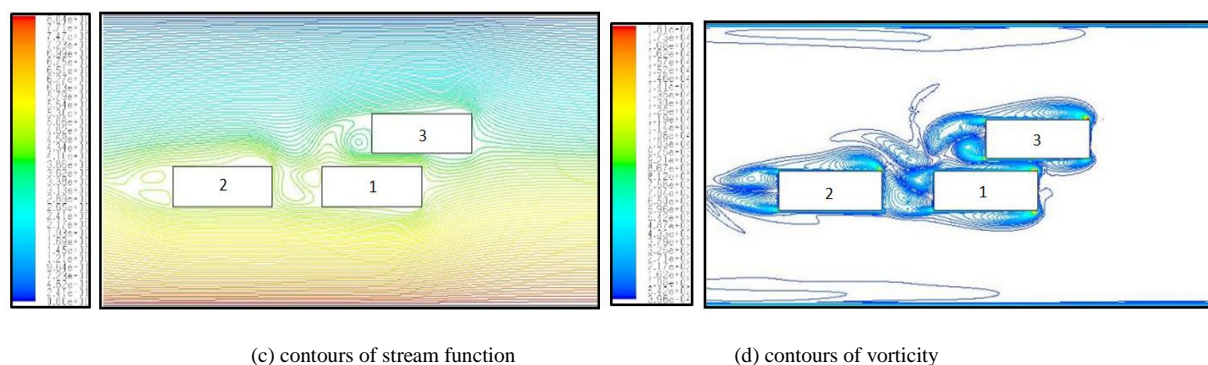


Figure 10. CFD simulation at  $U=20$  m/s ( $Re=55,120$ ),  $L/D=1.375$  and  $M/D=0.57$  of tandem three minibus cars in model IV configuration (a) contours of pressure, (b) contours of velocity magnitude, (c) contours of stream function and (d) contours of vorticity

Figs. 10 show a tandem of three minibus cars in configuration IV. In Fig. 10 (a), it can be seen that there is an increase of pressure on the front wall of car 1 and car 3, then a massive reduction on the left side of car 1 and car 3, while car 2 remains stable. In Fig. 10(b), the flow separation causes the boundary layer to be slightly pushed upwards, both on car 2 and car 3. It also shows quite intense vortices behind car 2 and car 3, as depicted in Fig. 10 (c) and Fig. 10 (d).

#### IV. CONCLUSIONS

Aerodynamic characteristics of four configurations of three tandem minibus models have been examined in terms of pressure coefficients and flow separation. The configurations are defined by the ratios of the relative distance of one car to the other two sequencing cars ( $M$ ), the distances of the two sequencing cars ( $L$ ), and the headway of the single one to the last car in the sequencing ones ( $N$ ) to the hydraulic diameter of the model ( $D$ ). There are six  $M/D$  ratios (0.57, 1.13, 1.70, 2.27, 2.84, and 3.41) and four  $N/D$  ratios (0.0, 2.75, 5.50, and 8.25) applied on models' arrangement, while the  $L/D$  ratio is fixed at 2.75. At fixed Reynolds number ( $Re$ ) 55,120, all models show considerably large differences in flow separation characteristics. The dominant optimum pressure coefficient is found to be positive. Consecutive small to large flow separations, characterized by flow vortex, occur at  $M/D=0.57$  in the following order: configuration III ( $N/D=5.50$ ), configuration II ( $N/D=2.75$ ), configuration I ( $N/D=0.0$ ), and configuration IV ( $N/D=8.25$ ).

#### CONFLICT OF INTEREST

The authors declare no conflict of interest.

#### AUTHOR CONTRIBUTIONS

Dr. N. Salam, main author, organized research promotion, conducted research planning. Dr. R. Tarakka, corresponding author, conducted research. Dr. Jalaluddin, conducted the research, Mr. MA. Jimran, conducted experimental research, and Mr. M. Ihsan, wrote and translated the manuscript. All authors have approved the final version.

#### ACKNOWLEDGMENTS

This research was funded through the 2020 University Basic Research (PDU) Scheme, the Unhas Rector's Decree Number 2649/UN4.1/KEP/2020, May 22, 2020, under the auspices Community Service Institute. The authors express their gratitude to the Head and Staff of the Fluid Mechanics Laboratory of the Hasanuddin University, Faculty of Engineering

#### REFERENCES

- [1] N. Salam, I.N.G. Wardana, S. Wahyudi, D. Widhiyanuriyawan, "Pressure distribution of fluid flow through triangular and square cylinders," *Aust. J. Basic & Appl. Sci.*, vol. 8, no. 3, pp. 263-267, 2014.
- [2] S. Kant, D.D. Srivastava, R. Shanker, R.K. Singh, and A. Sachan, "A review on CFD analysis of drag reduction of a generic sedan and hatchback," *International Research Journal of Engineering and Technology (IRJET)*, vol. 04, no. 05, 2017.
- [3] A.A. Moussa, R. Yadav, and J. Fischer, "Aerodynamic drag reduction for a generic sport utility vehicle using rear suction," *Journal of Engineering Research and Applications*, ISSN : 2248-9622, vol. 4, no. 8, (Version 7), pp. 101-107, 2014.
- [4] E.M. Wahba, H. Al-Marzooqi, M. Shaath, M. Shahin, and T. El-Dhmarshawy, "Aerodynamic drag reduction for ground vehicles using lateral guide vanes," *CFD Letters*, vol. 4, no. 2, pp. 68-79, 2012.
- [5] A.D. Lamond, J.J. Kennedy, and M. Stickland, "An investigation into unsteady base bleed for drag reduction in bluff two-box SUV's," in *Proc. 4th European Automotive Simulation Conference (EASC)*, Munich, Germany, (2009).
- [6] N. Salam, R. Tarakka, Jalaluddin, and R. Bachmid, "The effect of the addition of Inlet Disturbance Body (IDB) to flow resistance through the square cylinders arranged in tandem," *International Review of Mechanical Engineering (I.R.E.M.E.)*, vol. 11, no. 3, pp. 181-190, 2017.
- [7] W. Mokhtar and S.I. Jahan, "CFD study of aerodynamic flow around generic sports utility vehicle," in *Proc. the 2019 American Society for Engineering Education (ASEE) North Central Section Conference*, (2019).
- [8] S. Singh, M. Zunaid, N.A. Ansari, S. Bahirani, S. Dhall, and S. Kumar, *Numerical Study of the Generic Sports Utility Vehicle Design with a Drag Reduction Add-On Device*, Hindawi Publishing Corporation, Journal of Computational Engineering, Volume 2014, Article ID 785294, p. 17, 2014.
- [9] S.M.R. Hassan, T. Islam, M. Ali, M.Q. Islam, "Numerical study on aerodynamic drag reduction of racing cars," in *Proc. 10th International Conference on Mechanical Engineering, ICME 2013*, Procedia Engineering 90, pp. 308-313, 2014.

- [10] R. Tarakka, N. Salam, Jalaluddin, and M. Ihsan, "Active flow control by suction on vehicle models with variations on front geometry," *International Review of Mechanical Engineering (I.R.E.M.E.)*, vol. 12, no. 2, 2018.
- [11] F. Browand, *Reducing Aerodynamic Drag and Fuel Consumption*, Global Climate and Energy Project, Workshop on Advanced Transportation, Stanford University, (2005).
- [12] M. N. Sudin, M. A. Abdullah, S. A. Shamsuddin, F. R. Ramli, and M. M. Tahir, "Review of research on vehicles aerodynamic drag reduction methods," *International Journal of Mechanical & Mechatronics Engineering IJMME-IJENS*, vol. 14, no. 02, 2014.
- [13] B.Wang, Z. Yang, and H. Zhu, "Active flow control on the 25 ahmed body using a new unsteady jet," *International Journal of Heat and Fluid Flow*, vol. 79, 2019.
- [14] M. Roum ás, P. Gilli ón, and A. Kourta, "Drag reduction by flow separation control on a car after body," *International Journal for Numerical Methods in Fluids*, vol. 60, no. 11, pp. 1222-1240, 2009.
- [15] N. Salam, R. Tarakka, Jalaluddin, and M. Ihsan, "Flow separation across three square cylinders arranged in serial and parallel tandem configuration," *International Journal on Engineering Applications (I.R.E.A.)*, vol. 8, no. 3, pp. 96-106, 2020.
- [16] S. Aubrun, J. McNally, F. Alvi, and A. Kourta, "Separation flow control on a generic ground vehicle using steady microjet arrays," *Experiments in Fluids*, vol. 51, no. 5, pp.1177-1187, 2011.
- [17] E. Wassen, and F.H. Thiele., "Simulation of active separation control on a generic vehicle," in *Proc. 5th Flow Control Conference*, Chicago, Illinois, USA, 2010.
- [18] Y. A. Cengel, and J. M. Cimbala, *Fluid Mechanics Fundamentals and Applications*, Published by The Mc Graw-Hill Companies, Inc. New York (2006).
- [19] Plint & Partner LTD Engineer, *Manual Educational Wind Tunnel*, England (1982).



**Rustan Tarakka**—born in Pinrang on August 27<sup>th</sup> 1975 is an Associate Professor of Mechanical Engineering, Faculty of Engineering, Hasanuddin University, Makassar, Indonesia. He holds a doctoral degree from University of Indonesia, Jakarta, Indonesia. His research focuses fluid dynamics and computational fluid dynamics. Dr. Tarakka is a member of the Institutions of Engineers Indonesia.



**Jalaluddin**— was born in Sompu on August 25<sup>th</sup> 1972. He obtained a Doctor of Engineering in Mechanical Engineering in 2012 from Saga University Japan. He is an Associate Professor of Mechanical Engineering at Hasanuddin University, Makassar, Indonesia. His area of research covers Ground Heat Exchanger for Space Conditioning System, Renewable Energy with focus on Solar Energy including Solar Water Heating System and Photovoltaic Applications. Dr-Eng. Jalaluddin is a member of Institutions of Engineers Indonesia.



**Muh. Annur Jimran**— was born in Kadidi December 16<sup>th</sup> 1992. He graduated with a bachelor's degree from Automotive Engineering Education at the State University of Makassar. He is a postgraduate student in the Fluid Mechanics Laboratory, Department of Mechanical Engineering, Faculty of Engineering, Hasanuddin University, Makassar, Indonesia.



**Muhammad Ihsan** -born in Watampone, February 20<sup>th</sup> 1977, is a lecturer in Baramuli College of Engineering, Pinrang, Indonesia. He holds master degrees in transport engineering from Asian Institute of Technology, Bangkok, Thailand and Universitas Gajah Mada, Yogyakarta, Indonesia



**Nasaruddin Salam** – born in Bulukumba on December 20<sup>th</sup> 1959 is a Professor and the Chairman of Fluid Mechanics Laboratory in the Department of Mechanical Engineering, Faculty of Engineering, Hasanuddin University Makassar Indonesia. He holds a doctoral degree from Brawijaya University, Malang Indonesia. His research fields include fluid dynamics particularly on tandem bodies. Prof. Nasaruddin Salam is a member of the Institutions of Engineers Indonesia.